Effect of structural conformation of conjugated polymers on spin transport

Constantinos Nicolaides [1], Eliana Nicolaidou [2], Paris Papagiorgis [3], Grigorios Itskos [3],
Sophia C. Hayes [2], and Theodossis Trypiniotis [1,*]

[1]*Department of Physics, University of Cyprus, P.O. Box 20537, 1678 Nicosia, Cyprus*
[2]*Department of Chemistry, University of Cyprus, P.O. Box 20537, 1678 Nicosia, Cyprus*
[3]*Department of Physics, Experimental Condensed Matter Physics Laboratory, University of Cyprus,*
P.O. Box 20537, 1678 Nicosia, Cyprus

Organic semiconductors consisting mainly of relatively light chemical elements were expected to exhibit low spin-orbit coupling (SOC) and large spin relaxation time, making them attractive as spin conveyors in spintronic devices. However, a series of theoretical and experimental spin diffusion length and spin Hall angle results contradicting this expectation have triggered an ongoing discussion to understand the coupling of spins to their environment in these systems. In this context we use the prototype material poly(3,4-ethylenedioxythiophene):polystyrene sulfonate as a model conducting polymer system to monitor the impact of chemical doping and the resulting modification of the polymer's backbone conformation on the spin diffusion length. We observed an increase by a factor of 2 of the spin diffusion length during dedoping of the polymer that is accompanied by a respective order of magnitude decrease in the spin Hall angle and the spin admixture parameter indicating a reduction of the SOC strength. This trend is associated with an increased planarity at the dedoped level monitored by Raman spectroscopy revealing that spin transport is inextricably linked to the structural conformation of the organic semiconductor. Spin phenomena of a conjugated polymer can be modified through control of the polymer's structural conformation, paving the way for a new functionality for spintronic based devices.

I. INTRODUCTION

Organic semiconductors (OSCs) have been widely studied over the past few decades and a variety of technological applications have already been developed, such as organic light emitting diodes [1], solar cells [2,3], and organic transistors [4,5]. They have unique electrical, optical, and mechanical properties, which in combination with their ease of processing, low cost, and the wide range of different choices of structures makes them a particularly attractive category of materials for a wide variety of applications. Recently, there has been an emergence of organic spintronics studies, aiming to understand the spin relaxation and spin transport mechanisms in organic materials and to exploit their particular properties to invent new spintronic functionalities and devices [6,7].

The spin relaxation time, spin diffusion length (SDL), and spin Hall angle (θ_{SH}) are interconnected crucial figures of merit which determine the spin "conductivity" of a material and whether it is more suitable as a conveyor or a detector of spin. The spin relaxation time is controlled by two principal factors, the spin-orbit coupling (SOC) and the hyperfine interaction [6]. Since organic materials mainly consist of elements with small atomic numbers (e.g., H, C, O), very long spin

diffusion lengths and spin relaxation times are expected, with associated small spin Hall angles [8,9]. Many experimental reports, however, demonstrated spin diffusion lengths ranging from about 1 nm to approximately 1 μm in organic structures with similar light elements, which implies that in some cases the SOC strength is higher than expected [8,10–12].

The origin of such unexpected results is still under investigation and a detailed understanding of the mechanism of spin transport in these systems remains a very active research area both theoretically and experimentally [6,13,14]. The prominent candidate mechanisms proposed are spin transport mediated by spin-orbit coupled carrier hopping [13,15], or, at higher carrier concentrations, exchange coupling between localized carriers (polarons) [14,16]. There may not be a single valid mechanism for a specific OSC or even for the same OSC under different conditions, but rather a combination of the different mechanisms with one prevailing over the other in different circumstances [8,17].

Understanding a closely related property, the relaxation of spin in OSCs, is also crucial to enable spintronic applications of these materials. Recently, it has been proposed that at room (high) temperature in systems with incoherent charge transport, spin relaxation is governed by an Elliot-Yafet like mechanism [18]. The main characteristic is that instead of taking place during momentum scattering as in inorganic materials, the spin decay is caused by spatial scattering during charge hopping between mixed spin states with the admixture

*Corresponding author: theot@ucy.ac.cy

induced by the SOC [18–20]. The strength of the SOC is reflected in the spin-admixture parameter γ, which is a measure of the spin-flip probability during a hopping event. Theoretical calculations of γ have been performed by Yu [21,22] and more recently an accurate and more general formalism was introduced by Chopra *et al.* [19,20]. The conformation of the polymer structure is believed to affect γ since it depends on the relative orientation of neighboring π orbitals. More specifically, higher SOC is obtained for greater torsional angles along the polymer backbone of an OSC [12].

In this work, we aim to elucidate the link between a polymer's backbone conformation and SOC using poly(3,4-ethylenedioxythiophene):poly(4-styrenesulfonate), most commonly referred to as PEDOT:PSS, as a model material. We use chemical doping or dedoping, to alter the polymer's structural conformation and based on the framework developed by Yu, which refers to simultaneous spin transport through hopping and exchange coupling [8,17], we estimate the spin diffusion length of PEDOT:PSS for various degrees of doping by combining electron spin resonance (ESR) and Hall techniques. As the doping degree is reduced, the spin diffusion length is enhanced. A consistent observation is obtained via independent inverse spin Hall effect (ISHE) measurements induced by spin pumping from which θ_{SH} is determined at the various doping levels. The observed trends are attributed to the variation of the degree of torsion between conjugated units along the polymer backbone of PEDOT, with the structural conformation and associated change in planarity monitored via Raman spectroscopy. We finally estimate the spin-admixture parameter γ, and find that it reduces as the polymer planarity increases. Overall, our study demonstrates that within a large number of parameters affecting spin transport in polymers, structural conformation stands out as one of the most significant ones.

II. EXPERIMENTAL DETAILS

PEDOT:PSS has remarkable properties that range from mechanical flexibility, ease of processing, outstanding stability at environmental conditions, and excellent thermoelectric abilities, and is already used in a range of technological applications [23,24]. It is a robust conjugated polymer in which carrier concentration can be tuned through electrochemical or chemical doping, where the PSS counterion has a central role. PSS functions as both a dopant to compensate charges of the PEDOT cations and as a dispersant to form a stable dispersion in an aqueous solution in the presence of the hydrophobic PEDOT [24,25]. However, as for other organic semiconductors, a common problem is the small ionization fraction of the PSS, requiring a large amount of the dopant to generate a high carrier concentration. As a result, there is a large amount of nonionized dopants that can significantly increase the tunneling distance between PEDOT chains and hence reduce the rate of carrier hopping and the overall conductivity of pristine PEDOT:PSS [26]. This obstacle can be overcome by introducing an organic solvent with high solubility in water and high hydrophilicity, such as Dimethyl Sulfoxide (DMSO), which isolates uncoupled PSS, changes the film morphology, and improves the crystallinity resulting in a significant increase of

TABLE I. Labeling of the PEDOT:PSS samples in descending doping order with additive concentrations.

Sample ID	P1	P2	P3	P4	P5	P6
Additive	DMSO	–	NaOH	NaOH	NaOH	NaOH
Conc. (Vol %)	1	–	0.5	0.5	0.5	1
[NaOH] (M)		–	0.5	4	5	4

carrier concentration and conductivity [26–28]. The opposite outcome is achieved by the insertion of a dedopant, such as NaOH, that neutralizes PEDOT:PSS and disrupts the π conjugation of the PEDOT structure [29,30]. In order to have different degrees of doping for PEDOT:PSS we employed different amounts of DMSO or NaOH to respectively adjust the doping or dedoping of the polymer. The series of samples with different doping levels, labeled P1–P6, as used throughout this study, is presented in Table I. The ability to tune the doping level is confirmed by conductivity and carrier concentration measurements presented in Fig. 1 and further supported by optical absorbance measurements displayed in Fig. S1 of the Supplemental Material (SM) [31–34].

Experiments were carried out at room temperature using solution-processed PEDOT:PSS (PH1000, PEDOT:PSS ratio = 1:2.5) filtered using a 0.45-µm PVDF syringe filter as the starting material. The substrates were cleaned with deionized water and isopropanol in an ultrasonic bath and dried with nitrogen gas followed by UV-ozone treatment for 10 min before use. For Hall, spin pumping, conductivity, absorbance, and Seebeck measurements a volume of 20 µL of PEDOT:PSS solution was spin coated at 4000 rpm in ambient conditions and the resulting films were then annealed at 120 °C for 15 min. For ESR and Raman measurements the samples were prepared by drop-casting 5 and 20 µL of PEDOT:PSS solution, respectively, and dried at 120 °C for 20 min. Where needed Cu contact pads were thermally evaporated through a shadow mask. Conductivity measurements were carried out through a four-probe method. Additionally, for spin pumping and ESR measurements the samples were placed at the center of a TE_{102} rectangular cavity with an operational frequency of 9.43 GHz. The detailed experimental
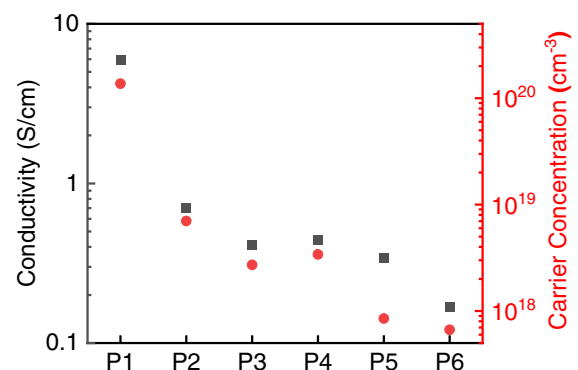

FIG. 1. Conductivity and carrier concentration for studied samples. Data arranged in increasing degree of dedoping.

procedures for the Hall, Seebeck, and Raman measurements can be found in the SM [31].

III. RESULTS AND DISCUSSION

A. Estimation of spin diffusion length

Spin transport in organic materials differs from inorganic structures, since spin carriers in an organic disordered film (polarons), although mobile, are usually localized, while transport in inorganic structures proceeds via delocalized Bloch waves. Consequently, in a regime with a large localized polaron concentration, exchange coupling is favored and as a result spin transport can be realized without charge transfer [14,16]. This exchange induced spin flow is not the only possible mechanism of spin transport. Polarons can also move through hopping which results in simultaneous spin and charge transport. Both of the above mechanisms influence the spin diffusion length (SDL) λ_N of an OSC and the spin relaxation time (T_1) can be related via the spin diffusion coefficient (D) through the classical Einstein relation $\lambda_N = \sqrt{D\,T_1}$, the validity of which has already been investigated in disordered OSCs theoretically [22] and experimentally [35]. The spin diffusion coefficient has two major contributions given by the relation

$$D = D_{\text{hop}} + D_{\text{exc}} = \mu k_B T/e + 1.6 J(R) R^2/\hbar. \quad (1)$$

The first term corresponds to the hopping contribution, where μ is the mobility, k_B is the Boltzmann constant, and e is the elementary charge. The second is the exchange-mediated contribution and is a function of the exchange interaction between neighboring polarons $J(R)$ and the average interpolaron distance R, which is related to polaron density (n) as $R = 1/\sqrt[3]{n}$. The exchange coupling can be estimated by a hydrogenic exchange interaction expression [8,17]

$$J(R) = 0.821 \frac{1}{4\pi\varepsilon\varepsilon_o} \left(\frac{e^2}{\xi}\right) \left(\frac{R}{\xi}\right)^{5/2} e^{-2R/\xi}, \quad (2)$$

where $\varepsilon = 2$ is the dielectric constant and ξ is the polaron localization length along the π-π stacking direction, which was experimentally obtained in a previous report to be equal to 11 nm for PEDOT:PSS [15]. For the evaluation of the SDL for every doping level, the mobility (μ), spin relaxation time (T_1), and polaron density (n) have to be experimentally estimated.

The conventional Hall-effect measurement method to obtain mobility and carrier concentration is often very challenging, since PEDOT:PSS is a disordered organic material with amorphous microstructure and high doping level and it is expected to produce small Hall voltage [36,37]. We surpassed this obstacle by utilizing a van der Pauw geometry with microscale four-finger electrode gap patterns and high DC magnetic field [38] (see further details in Sec. S2 of the SM [31]). The carrier concentration and mobility results are depicted in Figs. 1 and 2(a), respectively. During dedoping the carrier concentration is gradually decreased by approximately two orders of magnitude from 1.4×10^{20} to 6.7×10^{17} cm^{-3}. The mobility presents the opposite behavior,

decreasing for DMSO-treated PEDOT:PSS film and increasing for the NaOH-treated samples, in agreement with previous experimental reports [39,40].

The spin nature of charge carriers in PEDOT and other polythiophene-based organic materials under variable doping level can be determined through continuous wave ESR spectroscopy [18,41–43]. The ESR signal allows investigation of the spin dynamics of polarons, while at the same time acting as a spin counter for the determination of the polaron concentration in the sample under investigation. Figure 2(b) shows the ESR spectra for all samples at room temperature at constant microwave power. Every spectrum can be fitted by a single Lorentzian indicating that all the spins are in a homogeneous magnetic situation [9,15]. This fact means that the spin-spin relaxation (dephasing) time T_2 can be experimentally determined from the linewidth (ΔH_{FWHM}) by $T_2 = 2/\gamma_e \Delta H_{\text{FWHM}}$, where γ_e is the gyromagnetic ratio [44]. Furthermore, the doubly integrated spectra give the relative number of spins and by calibrating with the standard 2,2-diphenyl-1-picrylhydrazyl (DPPH) spin-1/2 radical we can obtain the polaron density (n) [Fig. 2(c)]. A considerable enhancement of the linewidth is observed as the doping increases and this broadening of the ESR linewidth is in agreement with previous experimental studies with electrochemical doping in thiophene-based organic materials [42,43]. In contrast, for dedoped PEDOT:PSS, polarons are more localized resulting in a narrowed ESR spectrum [41]. There is also a gradual decrease of polaron concentration as a function of doping [Fig. 2(c)] which contradicts the behavior observed in charge carrier concentration obtained via electrical measurements in Fig. 1. The polaron concentration is 1–2 orders greater than the charge concentration for the sample treated with DMSO. The difference between polaron and charge concentration can be interpreted by the presence of a "trapped polaron" population [45,46], which does contribute to the ESR intensity signal but not to the electrical measurements. Addition of DMSO causes a significant reduction of trapped polaron population while simultaneously leading to spinless bipolaron formation [42,43]. Consequently, trapped polarons, polarons, and bipolarons coexist in PEDOT:PSS, the populations of which are modified during doping.

As already mentioned, by calculating the ΔH_{FWHM} from the ESR line shape, the transverse spin relaxation or spin dephasing time T_2 can be estimated; however, for the calculation of the SDL, the parameter of interest is the longitudinal spin relaxation or spin lattice relaxation time T_1. This can be determined by measuring the saturation behavior of the ESR intensity as the microwave magnetic field is varied [9,47]. The inset of Fig. 2(b) shows the ESR intensity dependence as a function of microwave magnetic field for sample P2. A linear dependence is observed even for the highest microwave magnetic field used and this corresponds to the case where $T_1 \approx T_2$ [9,15]. Similar behavior is observed for all studied samples that indicates a universal relationship of $T_1 \approx T_2$ across all the doping range probed (see Sec. S3 in the SM [31]). The estimated spin lattice relaxation time is plotted in Fig. 2(c). With all relevant parameters determined, the spin diffusion length can be estimated [Fig. 2(d)]. A gradual
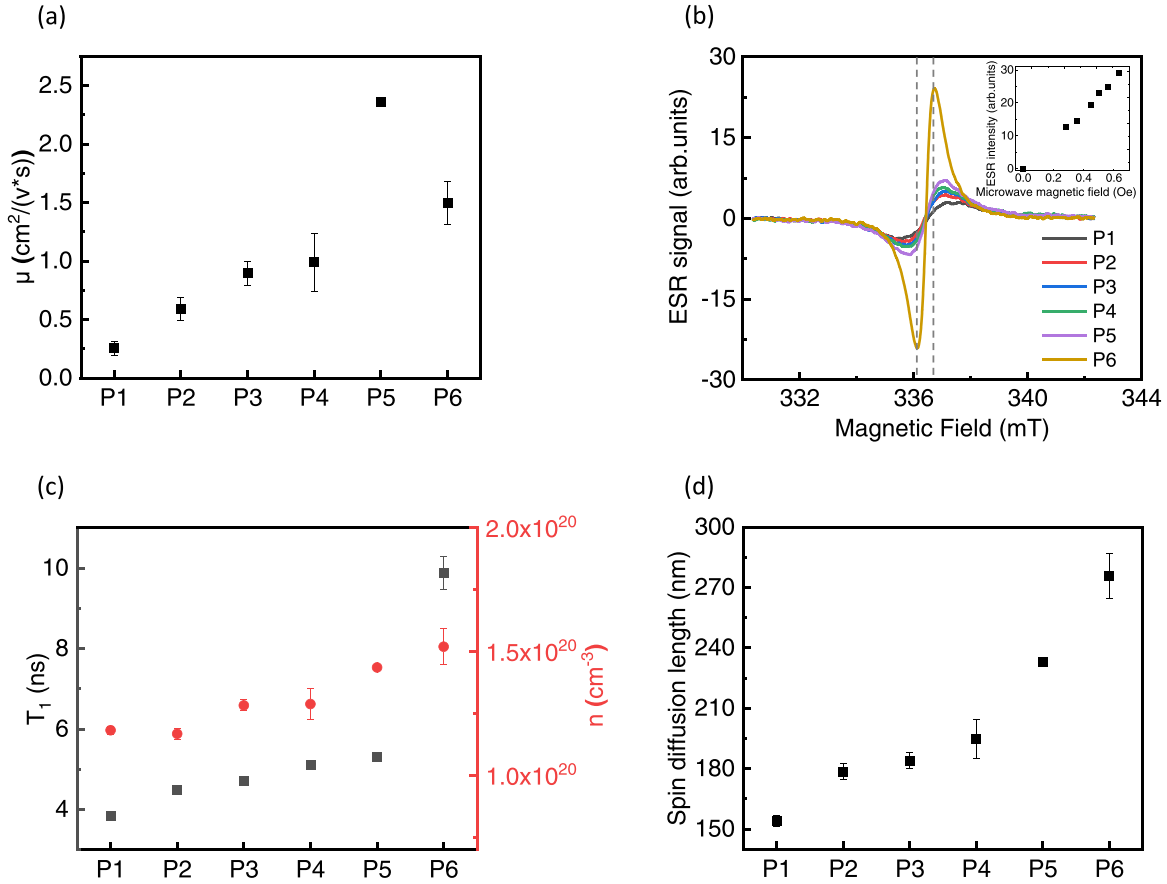
FIG. 2. (a) Mobility (μ) measurements plotted in increasing degree of dedoping from P1–P6. (b) ESR spectra of the PEDOT:PSS samples at different levels of chemical doping. The inset shows the microwave magnetic field dependence of the ESR intensity of the drop-casted pristine PEDOT:PSS film (P2) at room temperature. (c) Extracted spin relaxation time (T_1) and polaron concentration (n). (d) Estimated spin diffusion length (λ_N) for each sample obtained from ESR, Hall, and conductivity data.

increase of SDL is observed from higher to lower doping level, varying from ∼154 to ∼275 nm. The obtained values are in good agreement with previously reported measurements for PEDOT:PSS [15,48].

B. Estimation of spin Hall angle through ISHE measurements

In order to further probe the influence of doping on spin transport we have performed ISHE measurements, induced by spin pumping driven by ferromagnetic resonance (FMR) in a microwave cavity. We used a series of NiFe/PEDOT:PSS heterostructures with the same PEDOT:PSS doping levels, P1–P6. Figure 3(a) shows a schematic illustration of the device structure used for the ISHE experiments. The deposition sequence (NiFe and then spin coated PEDOT:PSS) was chosen in order to avoid the deposition of NiFe on the rough surface of PEDOT:PSS and therefore the increment of the damping term by extrinsic factors like inhomogeneity. A NiFe layer (7 nm) was deposited onto a Si/SiO$_X$ substrate by molecular beam epitaxy followed by a spin coated thin layer of PEDOT:PSS of approximately 80–90 nm (SM S4 [31]). During FMR, strong spin accumulation is induced by the precessing ferromagnet at the interface with the OSC and a pure spin current can be efficiently injected into the PEDOT:PSS layer. This excess of aligned spin-1/2 polarons along the mag-

netic field direction, which can be interpreted equivalently as spin angular momentum transfer from the ferromagnetic to the organic layer, can be detected as an electrical voltage utilizing the ISHE [49]. More specifically, in an organic material environment, the ISHE arises when (in the presence of SOC) in addition to hopping between pairs of sites, the hopping in a triad via an intermediate site gives rise to a nonzero phase shift for nonaligned molecular orientations of organic materials. This results in a charge imbalance in the direction perpendicular to the spin current and a corresponding induced electric field $\overrightarrow{E_{ISHE}}$ that can be detected electrically [48,50]. This process is phenomenologically described by the relation $\overrightarrow{E_{ISHE}} \propto \theta_{SH} \overrightarrow{J_S} \times \vec{\sigma}$, where $\overrightarrow{J_S}$ and $\vec{\sigma}$ are the spin current density and spin polarization, respectively. The parameter θ_{SH}, termed the spin Hall angle, describes the efficiency of the spin- to charge-current conversion process.

Figure 3(b) shows the voltage signal measured in the NiFe/P2 bilayer device under 62.8 mW microwave excitation power. The detected voltage can be fitted using the relation

$$V(H) = V_{Sym} \frac{\Delta H_{FWHM}^2}{(H - H_{FMR})^2 + \Delta H_{FWHM}^2}$$
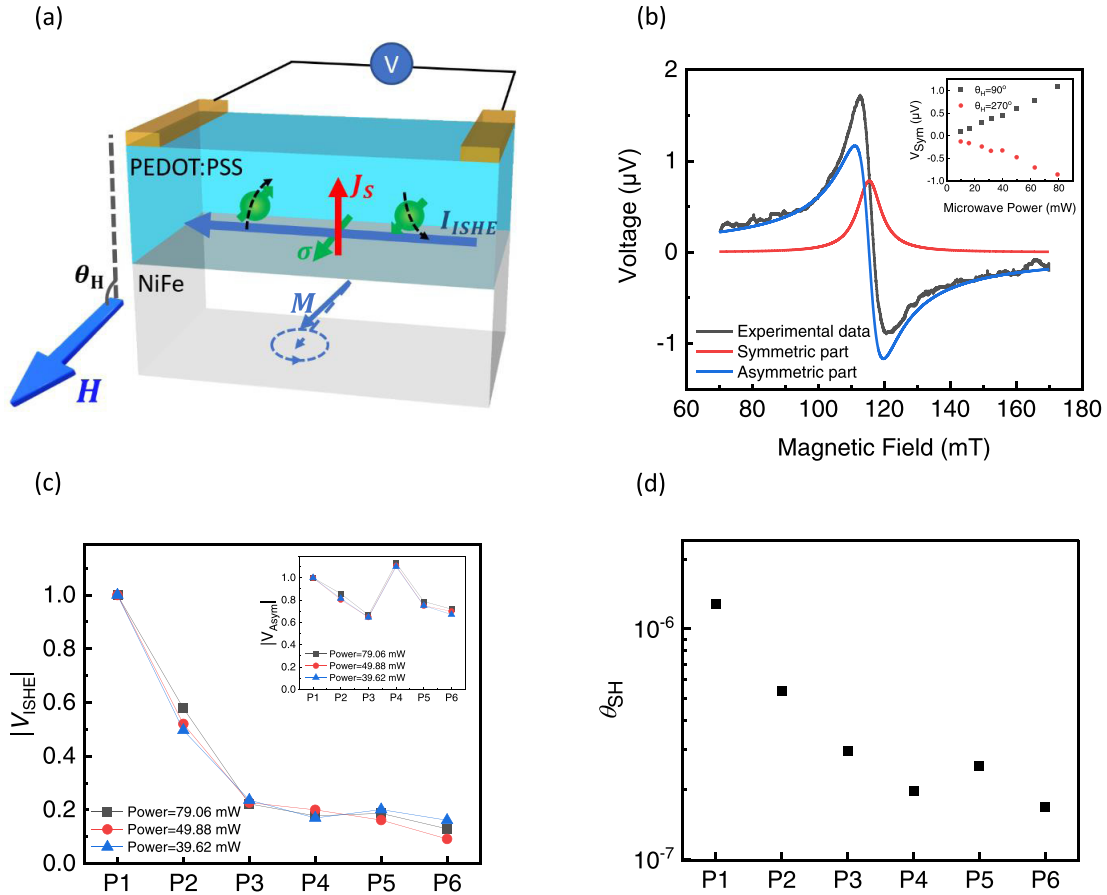$$+ V_{Asym} \frac{-2 \Delta H_{FWHM}(H - H_{FMR})}{(H - H_{FMR})^2 + \Delta H_{FWHM}^2}, \quad (3)$$

FIG. 3. (a) Schematic of the inverse spin Hall effect induced by the spin pumping in a NiFe/PEDOT:PSS bilayer device. H and θ_{H} denote the external magnetic field and the angle of H from sample plane, respectively. I_{ISHE}, j_{s}, σ denote the ISHE current due to spin-charge conversion, the flow direction of the spin current, and the spin-polarization vector, respectively. (b) Voltage signal detected in the NiFe/P2 bilayer, at $\theta_{\mathrm{H}} = 90°$ (black line) and the fitted symmetric (red line) and asymmetric part (blue line). The inset shows the microwave power dependence of the peak symmetric voltage for opposing in-plane orientations of the external magnetic field, $\theta_{\mathrm{H}} = 90°$ and $\theta_{\mathrm{H}} = 270°$. (c) $|V_{\mathrm{ISHE}}|$ measurements for each sample, for three different microwave powers, where $|V_{\mathrm{ISHE}}|$ stands for the average of the symmetric voltage for opposing in-plane orientations of the external magnetic field, divided by the absorbed microwave intensity at FMR and normalized by the magnitude of P1. The inset shows the corresponding measurements for the asymmetric part of the voltage. (d) Estimation of spin Hall angle (θ_{SH}) from ISHE measurements.

where ΔH_{FWHM} and H_{FMR} are the linewidth and the ferromagnetic resonance field, respectively [51]. The first term describes the symmetric contribution to the voltage signal from the ISHE, while the second term corresponds to the asymmetric contribution, which is the result of different effects including the anomalous Hall effect and the anisotropic magnetoresistance [52,53]. The ISHE voltage exhibits a polarity change when measured at two opposite in-plane magnetic field directions, $\theta_{\mathrm{H}} = 90°$ and $\theta_{\mathrm{H}} = 270°$, in combination with a linear dependence of its magnitude on microwave power [inset of Fig. 3(b)], indicating the successful creation of ISHE voltage induced by spin pumping [54]. The results of the above SHE analysis for all samples are shown in Fig. 3(d). $|V_{\mathrm{ISHE}}|$ stands for the average of V_{ISHE} for opposing in-plane orientations of the external magnetic field, divided by the absorbed microwave intensity at FMR, P_{abs}, and normalized by the magnitude of P1. There is a clear gradual reduction of the $|V_{\mathrm{ISHE}}|$ from the higher doped level P1 to the lower doped

level P6. This tendency concerns only the symmetric part of voltage since the asymmetric part presents a different trend for the same doping levels [inset of Fig. 3(c)].

As has been discussed widely in the literature the symmetric voltage can be affected by thermoelectric effects [48,53]. In order to exclude this contribution to $|V_{\mathrm{ISHE}}|$ we measured the Seebeck coefficient (see SM Sec. S5 for results and experimental details [31]). The introduction of NaOH results in an increase of the Seebeck coefficient [Fig. S5(b) [31]] in agreement with other experimental studies [40,55] whereas the change in the symmetric contribution of the voltage decreases monotonically. After clarifying that the symmetric contribution of the voltage corresponds to the V_{ISHE} induced by the spin pumping process, we can estimate the spin Hall angle (θ_{SH}) for every doping level of PEDOT:PSS layer by [54]

$$V_{\mathrm{ISHE}} = \frac{w\theta_{\mathrm{SH}}\lambda_{\mathrm{N}}\tanh(d_{\mathrm{N}}/2\lambda_{\mathrm{N}})}{d_{\mathrm{N}}\sigma_{\mathrm{N}} + d_{\mathrm{F}}\sigma_{\mathrm{F}}}(2e/\hbar)j_{\mathrm{s}}^{o}, \qquad (4)$$

where w is the width of the NiFe layer between the Cu contacts, j_s^o is the spin current density, d_N, σ_N, d_F, and σ_F are the thickness and the conductivity of the PEDOT:PSS layer and the NiFe layer, respectively. θ_{SH} can be estimated (see detailed description in SM Sec. S6 [31]) for every doping level and the results are presented in Fig. 3(d). A gradual enhancement of spin Hall angle by one order (10^{-7}–10^{-6}) is observed during doping. The magnitude of the θ_{SH} is comparable with other reported work for PEDOT:PSS [48–50]. The change in θ_{SH} with doping is consistent with the variation of the SDL measured in Fig. 2(d) as the θ_{SH} should be inversely proportional to SDL [54].

C. Estimation of γ^2 and qualitative confirmation of PEDOT:PSS backbone conformation through resonance Raman measurements

There are two key findings from the above results from ESR and ISHE measurements: the increase of SDL during chemical dedoping of PEDOT:PSS and the associated reduction of θ_{SH}, both indicating that the degree of doping is associated with changes in the SOC strength. Since the doping procedure does not affect the atomic composition, we expect that the variation of the SOC originates in a possible alteration of the PEDOT's structural conformation upon doping. Indeed, the interplay between changes of the polymer's backbone conformation and chemical doping has been widely reported for OSCs [56–58]. In such situations, the strength of the SOC can be conveniently parametrized via the spin-admixture parameter, which is directly proportional to the ratio of spin flipping to spin-conserving hopping events [19,20,22]. The magnitude of γ^2 is expected to be maximized for large thiophene-thiophene dihedral angles (orthogonal π-orbitals) and minimized for a planar backbone PEDOT [21]. We can estimate γ^2 for every PEDOT:PSS doping level using the theory proposed by Wang *et al.* [8]. The spin-lattice relaxation time T_1 that is already obtained is affected by two principal contributions, SOC and hyperfine interaction (HFI), and is given by the relation

$$T_1 = (\omega_{HFI} + \omega_{SOC})^{-1} = \left(2\Omega_{HFI}^2 \tau/3 + 8\,\gamma^2/3\tau\right)^{-1}. \quad (5)$$

The spin relaxation rate due to the local HFI corresponds to the first term and $\Omega_{HFI} = 2\times10^8$ Hz is the Larmor frequency of the local hyperfine magnetic field, while the second corresponds to the spin relaxation rate due to the SOC. The dwell time τ of a spin on a molecule is given by $\tau = (2D_{hop}/\alpha^2 + 2D_{exc}/R^2)^{-1}$ where $\alpha = 0.37$ nm [28] is the average hopping distance between polarons along the π-π stacking direction. Figure 4(a) shows the estimate of γ^2 for every sample. A clear gradual reduction of the spin admixture is observed during dedoping with an overall decline of approximately one order of magnitude (10^{-6}–10^{-5}), indicating that the PEDOT backbone becomes more planar with the insertion of NaOH. Furthermore, the absolute values of γ^2 obtained are in good agreement with the theoretical estimation for sexithiophene (T_6), shown in Fig. 4(a) as a blue dashed line for comparison, whose structure is similar with PEDOT:PSS [21,50].

We can experimentally verify the above conclusion via resonance Raman spectroscopy, which can provide information regarding the structural conformation of conjugated polymers. In a typical resonance Raman spectrum of PEDOT:PSS, four main peaks are distinguished [39,59,60]. Two of them are ascribed to the stretching modes of inter- and intra-ring C–C single bonds of thiophene, centered at ~1250 and ~1360 cm^{-1}, and the other two to the symmetric and asymmetric stretches of C = C double bonds at ~1430 and 1520 cm^{-1}, respectively. The most significant changes observed during the dedoping process are identified in the Raman band between 1400 and 1500 cm^{-1}, which is mainly due to C = C symmetric stretching. This band includes contributions from the symmetric stretching modes of the C_α–C_β(–O) bond in the quinoid structure and the C_α = C_β(–O) bond in the benzoid structure at ~1430 and ~ 1450 cm^{-1}, respectively, and the asymmetric C_α = C_β(–O) stretching at 1400 cm^{-1} [39]. The quinoid structure represents a more linear backbone with enhanced planarity, stemming from the double bond C_α = $C_{\alpha'}$ between the thiophene units, which locks the backbone dihedral angle to 180°, while the benzoid structure has a favored coil conformation, as the single bond C_α–$C_{\alpha'}$ facilitates inter-ring twisting [Fig. 4(c)] [56]. Consequently, Raman spectroscopy gives the opportunity for an in-depth understanding of PEDOT's structural change during chemical doping, by tracking the quinoid/benzoid ratio for every sample. Figure 4(b) shows the Raman spectra with 532-nm excitation for every doping level. At high doping levels the C = C symmetric stretch band is broader, reflecting the conformational disorder of the polymer in mixed charge states (neutral, polaron, and bipolaron). The shorter conjugation length of the neutral benzoid segments at these doping levels shifts the benzoid band to higher wavenumbers with enhanced contribution (see SM Sec. S7, Fig. S8 [31]) [61,62]. A clear shift of the position of the C = C symmetric stretch band to lower wavenumbers is observed upon dedoping. This is more prominent in the Raman spectrum of P6, with a downshift of 7 cm^{-1} of the quinoid C = C stretch band, which in combination with the pronounced narrowing of the C = C linewidth (full width at half maximum), constitutes a distinct signature of the increased planarity of PEDOT's backbone expected for the quinoid conformation [61,63]. This tendency of the resonance Raman spectra is in agreement with the corresponding behavior of Raman spectra during electrochemical and chemical doping or dedoping reported previously [61,64]. Moreover, the appropriate deconvolution of the C = C symmetric stretch peak shown in Fig. 4(c) (see SM Sec. S7 for analysis [31]) further confirms the gradual enhancement of the quinoid, more planar, structure when dedoped and especially its predominance in the case of P6, which along with its narrower linewidth indicates a smaller distribution of PEDOT structural conformations [Fig. 4(c)] [61].

To sum up, the spin admixture parameter γ^2 was obtained after taking into consideration the effect of the doping/dedoping process on all relevant parameters affecting it, i.e., spin relaxation time, mobility, and polaron concentrations. An increase by one order of magnitude in γ^2 during dedoping suggests weaker SOC strength. This is
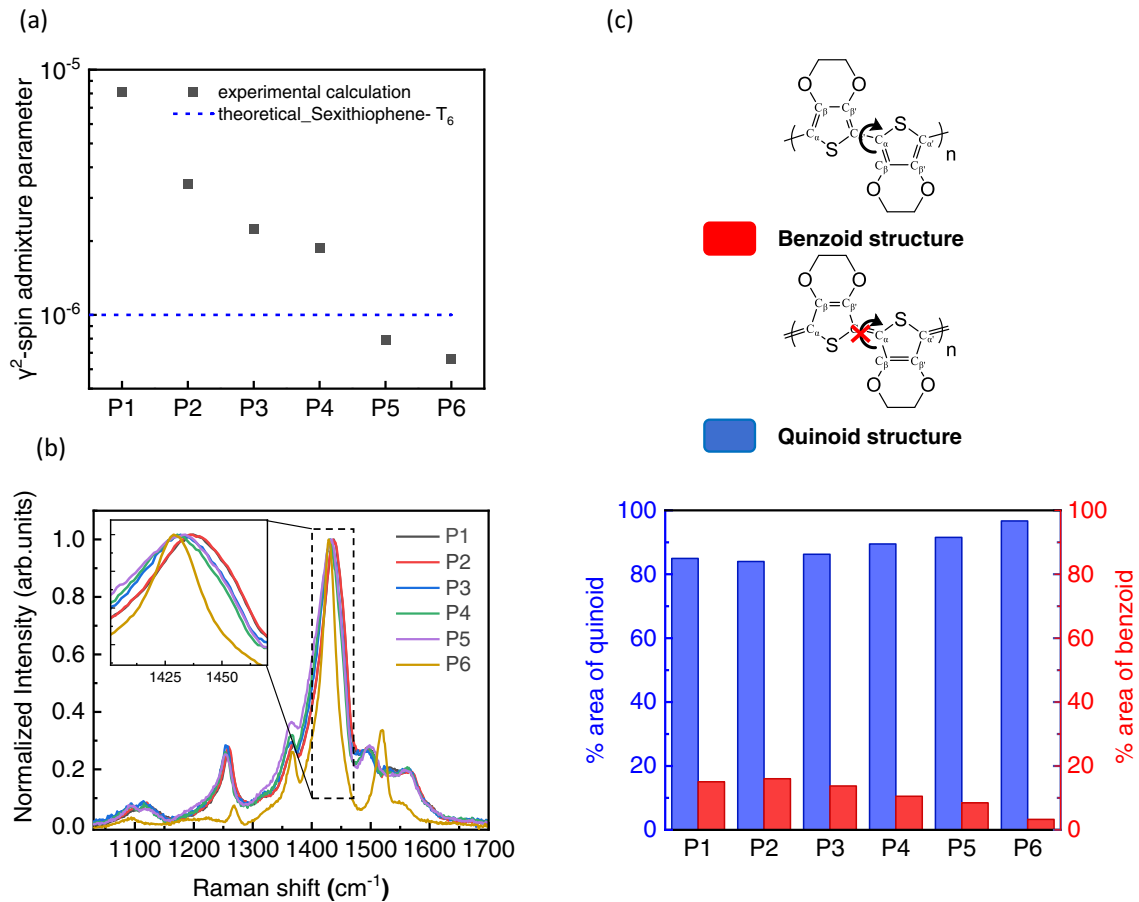
FIG. 4. (a) Estimation of the spin admixture parameter γ^2 for P1–P6. For comparison, we plot the theoretical value of sexithiophene (T_6) (blue dashed line) a material with linear conformation and very similar structure with PEDOT [17,21]. (b) Normalized resonance Raman spectra of the PEDOT:PSS samples at different doping levels with excitation at 532 nm. (c) Percentage of the quinoid and benzoid band within our different samples obtained from Raman data deconvolution together with the corresponding structures.

consistent with the experimental confirmation of increased planarity for lower doping through Raman measurements. The resulting reduction in SOC and therefore, lower probability for spin-flip during hopping is consistent with the longer spin diffusion length or smaller spin Hall angle observed. Consequently, chemical doping becomes a control factor of spin diffusion length, while Raman spectroscopy can be a sensitive detection tool to trace it indirectly.

IV. CONCLUSION

We have explored the influence of structural conformation of conjugated polymer on spin transport in PEDOT:PSS at different chemically defined doping levels. The spin diffusion length obtained varies from 154 to 275 nm with increasing dedoping corresponding to gradual reduction of the spin admixture parameter γ^2 by one order of magnitude and therefore an associated SOC strength reduction. A similar trend is observed by an associated decrease of the spin Hall an-

gle θ_{SH}, estimated through ISHE measurements induced by FMR-spin pumping. Since the chemical composition of the organic semiconductor remains the same by the doping procedure, we attribute the change of the SOC strength to the alteration of the structural conformation of the polymer. This is confirmed through resonance Raman spectroscopy with the predominance of the more planar quinoid structure at lower doping levels, indicating that enhanced planarity is associated with SOC strength reduction. This study offers an intrinsic way of controlling SOC by manipulating the OSC's structural conformation, which can be used for future spin transport studies in these materials as well as to enhance functionality in spintronic devices.

[1] J. H. Burroughes, D. D. C. Bradley, A. R. Brown, R. N. Marks, K. Mackay, R. H. Friend, P. L. Burns, and A. B. Holmes, Nature (London) **347**, 539 (1990).

[2] A. J. Heeger, Adv. Mater. **26**, 10 (2014).

[3] J. Zhao, Y. Li, G. Yang, K. Jiang, H. Lin, H. Ade, W. Ma, and H. Yan, Nat. Energy **1**, 15027 (2016).

[4] J. Lenz, F. del Giudice, F. R. Geisenhof, F. Winterer, and R. T. Weitz, Nat. Nanotechnol. **14**, 579 (2019).

[5] U. Zschieschang and H. Klauk, J. Mater. Chem. C **7**, 5522 (2019).

[6] L. Guo, Y. Qin, X. Gu, X. Zhu, Q. Zhou, and X. Sun, Front. Chem. **7**, 428 (2019).

[7] V. A. Dediu, L. E. Hueso, I. Bergenti, and C. Taliani, Nat. Mater. **8**, 707 (2009).

[8] S. J. Wang, D. Venkateshvaran, M. R. Mahani, U. Chopra, E. R. McNellis, R. Di Pietro, S. Schott, A. Wittmann, G. Schweicher, M. Cubukcu, K. Kang, R. Carey, T. J. Wagner, J. N. M. Siebrecht, D. P. G. H. Wong, I. E. Jacobs, R. O. Aboljadayel, A. Ionescu, S. A. Egorov, S. Mueller *et al.*, Nat. Electron. **2**, 98 (2019).

[9] J. Tsurumi, H. Matsui, T. Kubo, R. Häusermann, C. Mitsui, T. Okamoto, S. Watanabe, and J. Takeya, Nat. Phys. **13**, 994 (2017).

[10] D. Sun, K. J. Van Schooten, M. Kavand, H. Malissa, C. Zhang, M. Groesbeck, C. Boehme, and Z. V. Vardeny, Nat. Mater. **15**, 863 (2016).

[11] S. Watanabe, K. Ando, K. Kang, S. Mooser, Y. Vaynzof, H. Kurebayashi, E. Saitoh, and H. Sirringhaus, Nat. Phys. **10**, 308 (2014).

[12] E. Vetter, I. Vonwald, S. Yang, L. Yan, S. Koohfar, D. Kumah, Z.-G. Yu, W. You, and D. Sun, Phys. Rev. Mater. **4**, 085603 (2020).

[13] Q. Lu, S. Xie, and F. Qu, J. Phys. Chem. Lett. **12**, 3540 (2021).

[14] Q. Lu, S. Yin, T. Gao, W. Qin, S. Xie, F. Qu, and A. Saxena, J. Phys. Chem. Lett. **11**, 1087 (2020).

[15] M. Kimata, D. Nozaki, Y. Niimi, H. Tajima, and Y. C. Otani, Phys. Rev. B **91**, 224422 (2015).

[16] S. W. Jiang, S. Liu, P. Wang, Z. Z. Luan, X. D. Tao, H. F. Ding, and D. Wu, Phys. Rev. Lett. **115**, 086601 (2015).

[17] Z. G. Yu, Phys. Rev. Lett. **111**, 016601 (2013).

[18] S. Schott, U. Chopra, V. Lemaur, A. Melnyk, Y. Olivier, R. Di Pietro, I. Romanov, R. L. Carey, X. Jiao, C. Jellett, M. Little, A. Marks, C. R. McNeill, I. McCulloch, E. R. McNellis, D. Andrienko, D. Beljonne, J. Sinova, and H. Sirringhaus, Nat. Phys. **15**, 814 (2019).

[19] U. Chopra, S. Shambhawi, S. A. Egorov, J. Sinova, and E. R. Mcnellis, Phys. Rev. B **100**, 134410 (2019).

[20] U. Chopra, S. A. Egorov, J. Sinova, and E. R. McNellis, J. Phys. Chem. C **123**, 19112 (2019).

[21] Z. G. Yu, Phys. Rev. Lett. **106**, 106602 (2011).

[22] Z. G. Yu, Phys. Rev. B **85**, 115201 (2012).

[23] N. Kim, I. Petsagkourakis, S. Chen, M. Berggren, X. Crispin, M. P. Jonsson, and I. Zozoulenko, *Electric Transport Properties in PEDOT Thin Films* (CRC Press, Boca Raton, 2019).

[24] A. Elschner, S. Kirchmeyer, W. Lovenich, U. Merker, and K. Reuter, *PEDOT: Principles and Applications of an Intrinsically Conductive Polymer* (CRC Press, Boca Raton, 2010).

[25] B. G. Heywang and F. Jonas, Adv. Mater. **4**, 116 (1992).

[26] G. Kim, L. Shao, K. Zhang, and K. P. Pipe, Nat. Mater. **12**, 719 (2013).

[27] X. Crispin, F. L. E. Jakobsson, A. Crispin, P. C. M. Grim, P. Andersson, A. Volodin, C. Van Haesendonck, M. Van Der Auweraer, W. R. Salaneck, and M. Berggren, Chem. Mater. **18**, 4354 (2006).

[28] O. Bubnova, Z. U. Khan, H. Wang, S. Braun, D. R. Evans, M. Fabretto, P. Hojati-Talemi, D. Dagnelund, J.-B. Arlin, Y. H. Geerts, S. Desbief, D. W. Breiby, J. W. Andreasen, R. Lazzaroni, W. M. Chen, I. Zozoulenko, M. Fahlman, P. J. Murphy, M. Berggren, and X. Crispin, Nat. Mater. **13**, 190 (2014).

[29] Y. Mochizuki, T. Horii, and H. Okuzaki, Trans. Mater. Res. Soc. Jpn. **37**, 307 (2012).

[30] T.-C. Tsai, H.-C. Chang, C.-H. Chen, Y.-C. Huang, and W.-T. Whang, Org. Electron. **15**, 641 (2014).

[31] See Supplemental Material at http://link.aps.org/supplemental/10.1103/PhysRevMaterials.6.095601 for extended experimental methods, additional spectral data, and brief discussion regarding estimation of spin Hall angle.

[32] G. Rebetez, O. Bardagot, J. Affolter, J. Réhault, and N. Banerji, Adv. Funct. Mater. **32**, 2105821 (2021).

[33] B. D. Paulsen, R. Wu, C. J. Takacs, H. Steinrück, J. Strzalka, Q. Zhang, M. F. Toney, and J. Rivnay, Adv. Mater. **32**, 2003404 (2020).

[34] I. Zozoulenko, A. Singh, S. K. Singh, V. Gueskine, X. Crispin, and M. Berggren, ACS Appl. Polym. Mater. **1**, 83 (2019).

[35] G. A. H. Wetzelaer, L. J. A. Koster, and P. W. M. Blom, Phys. Rev. Lett. **107**, 066605 (2011).

[36] K. Kang, S. Watanabe, K. Broch, A. Sepe, A. Brown, I. Nasrallah, M. Nikolka, Z. Fei, M. Heeney, D. Matsumoto, K. Marumoto, H. Tanaka, S. I. Kuroda, and H. Sirringhaus, Nat. Mater. **15**, 896 (2016).

[37] Q. Wei, M. Mukaida, Y. Naitoh, and T. Ishida, Adv. Mater. **25**, 2831 (2013).

[38] S. Ozaki, Y. Wada, and K. Noda, Synth. Met. **215**, 28 (2016).

[39] L. M. Yu, T. Chen, N. Feng, R. Wang, T. Sun, Y. Zhou, H. Wang, Y. Yang, and Z. H. Lu, Sol. RRL **4**, 1900513 (2020).

[40] T. A. Yemata, Y. Zheng, A. K. K. Kyaw, X. Wang, J. Song, W. S. Chin, and J. Xu, RSC Adv. **10**, 1786 (2020).

[41] A. Zykwinska, W. Domagala, and M. Lapkowski, Electrochem. Commun. **5**, 603 (2003).

[42] D. Neusser, C. Malacrida, M. Kern, Y. M. Gross, J. Van Slageren, and S. Ludwigs, Chem. Mater. **32**, 6003 (2020).

[43] A. V. Volkov, S. K. Singh, E. Stavrinidou, R. Gabrielsson, J. F. Franco-Gonzalez, A. Cruce, W. M. Chen, D. T. Simon, M. Berggren, and I. V. Zozoulenko, Adv. Electron. Mater. **3**, 1700096 (2017).

[44] C. P. Poole and H. A. Farach, *Relaxation in Magnetic Resonance* (Academic Press, New York, 1971).

[45] A. Privitera, R. Warren, G. Londi, P. Kaienburg, J. Liu, A. Sperlich, A. E. Lauritzen, and O. Thimm, J. Mater. Chem. C **9**, 2944 (2021).

[46] Y. Sakurai, D. Matsumoto, and K. Marumoto, Appl. Magn. Reson. **49**, 767 (2018).

[47] S. Schott, E. R. McNellis, C. B. Nielsen, H. Y. Chen, S. Watanabe, H. Tanaka, I. McCulloch, K. Takimiya, J. Sinova, and H. Sirringhaus, Nat. Commun. **8**, 15200 (2017).

[48] M. M. Qaid, M. R. Mahani, J. Sinova, and G. Schmidt, Phys. Rev. Res. **2**, 013207 (2020).

[49] K. Ando, S. Watanabe, S. Mooser, E. Saitoh, and H. Sirringhaus, Nat. Mater. **12**, 622 (2013).

[50] Z. G. Yu, Phys. Rev. Lett. **115**, 026601 (2015).

[51] E. Saitoh, M. Ueda, H. Miyajima, and G. Tatara, Appl. Phys. Lett. **88**, 182509 (2006).

[52] J. Lustikova, Y. Shiomi, and E. Saitoh, Phys. Rev. B **92**, 224436 (2015).

[53] R. Iguchi and E. Saitoh, J. Phys. Soc. Jpn. **86**, 011003 (2017).

[54] K. Ando, S. Takahashi, J. Ieda, Y. Kajiwara, H. Nakayama, T. Yoshino, K. Harii, Y. Fujikawa, M. Matsuo, S. Maekawa, and E. Saitoh, J. Appl. Phys. **109**, 103913 (2011).

[55] Z. Fan, P. Li, D. Du, and J. Ouyang, Adv. Energy Mater. **7**, 1602116 (2017).

[56] X. Li, R. Zou, Z. Liu, J. Mata, B. Storer, Y. Chen, W. Qi, Z. Zhou, and P. Zhang, Npj Flex. Electron. **6**, 6 (2022).

[57] A. E. Mansour, A. M. Valencia, D. Lungwitz, B. Wegner, N. Tanaka, Y. Shoji, T. Fukushima, A. Opitz, C. Cocchi, and N. Koch, Phys. Chem. Chem. Phys. **24**, 3109 (2022).

[58] J. Gao, B. W. Stein, A. K. Thomas, J. A. Garcia, J. Yang, M. L. Kirk, and J. K. Grey, J. Phys. Chem. C **119**, 16396 (2015).

[59] S. Funda, T. Ohki, Q. Liu, J. Hossain, Y. Ishimaru, K. Ueno, and H. Shirai, J. Appl. Phys. **120**, 033103 (2016).

[60] S. Garreau, J. L. Duvail, and G. Louarn, Synth. Met. **125**, 325 (2001).

[61] E. Tan, A. M. Pappa, J. Nightingale, S. Wood, F. A. Castro, and J. S. Kim, Biotechnol. Bioeng. **117**, 291 (2019).

[62] S. Sakamoto, M. Okumura, Z. Zhao, and Y. Furukawa, Chem. Phys. Lett. **412**, 395 (2005).

[63] W. C. Tsoi, D. T. James, J. S. Kim, P. G. Nicholson, C. E. Murphy, D. D. C. Bradley, J. Nelson, and J. Kim, J. Am. Chem. Soc. **133**, 9834 (2011).

[64] M. Łapkowski and A. Proń, Synth. Met. **110**, 79 (2000).